Nano Energy 52 (2018) 510–516

Contents lists available at ScienceDirect

Nano Energy

journal homepage: www.elsevier.com/locate/nanoen

Full paper

Structural and electrochemical properties of $LiMn_{0.6}Fe_{0.4}PO_4$ as a cathode material for flexible lithium-ion batteries and self-charging power pack

Shaoqing Li[a,b], Xiaoyi Meng[a,b], Qiang Yi[a,b], José Antonio Alonso[d,*], M.T. Fernández-Díaz[e], Chunwen Sun[a,b,c,**], Zhong Lin Wang[a,b,c,f,**]

[a] CAS Center for Excellence in Nanoscience, Beijing Institute of Nanoenergy and Nanosystems, Chinese Academy of Sciences, Beijing 100083, PR China
[b] College of Nanoscience and Technology, University of Chinese Academy of Sciences, Beijing 100049, PR China
[c] Center on Nanoenergy Research, School of Physical Science and Technology, Guangxi University, Nanning 530004, PR China
[d] Instituto de Ciencia de Materiales de Madrid, CSIC, Cantoblanco, 28049 Madrid, Spain
[e] Institut Laue Langevin, BP 156X, Grenoble Cedex, France
[f] School of Material Science and Engineering, Georgia Institute of Technology, Atlanta, GA 30332-0245, USA

ARTICLE INFO

Keywords:
Flexible lithium-ion batteries
$LiMn_{0.6}Fe_{0.4}PO_4$
Neutron diffraction
Quasi-solid electrolyte
Triboelectric nanogenerators

ABSTRACT

Cathode materials with low-cost, environment-friendly, high energy density are critical for lithium-ion batteries (LIBs). Here, the effects of Fe doping on the structure of $LiMnPO_4$ (LMP) are investigated by neutron powder diffraction (NPD). The prepared $LiMn_{0.6}Fe_{0.4}PO_4$/carbon (LMFP/C) shows a higher specific capacity of 90 mAh g^{-1} at a current density of 1 C, which is about 5 times of that of $LiMnPO_4$/C. It also shows excellent cycling performance for 1000 cycles. The improved electrochemical performance is ascribed to the higher octahedral distortion of (Mn, Fe)O_6 and an easiness for Li diffusion due to much less anisotropic ellipsoids for Li in LMFP. We further fabricated a flexible LIB with LMFP/C cathode and an in-situ polymerized electrolyte, which exhibits excellent flexibility and cyclability. The cell shows no obvious performance degradation after bending for 300 times. Moreover, a flexible triboelectric nanogenerator (TENG) was coupled with the flexible cell to form a wearable self-charging power pack. The TENG can harvest mechanical energy and convert it into electrical form, charge the battery to supply energy for a flexible electrochromic membrane. The open circuit voltage (V_{OC}) of the flexible LIB increases from 3.32 V to 3.51 V in about 20 min through daily human motion.

1. Introduction

Flexible electronics are emerging, such as wearable devices, roll-up displays, electronic skins, and smart sensors [1–5]. To achieve full flexibility, a flexible energy storage system is highly needed. Among various kinds of energy storage devices, lithium ion batteries (LIBs) are believed as one of the best choices for portable electronics due to their high energy density and good cyclability [6,7]. However, the traditional LIBs are rigid, thus not compatible with flexible electronics. The current collectors, electrolyte and packaging should be optimized to achieve good performance under deformation [8–10].

$LiFePO_4$ (LFP) has become a successful cathode material since it was first reported by Goodenough et al. [11,12]. However, the power density of LFP cathode based cells cannot meet the expectation of some high-power systems. $LiMnPO_4$ (LMP) is a promising candidate to replace LFP as cathode for next generation LIBs, owing to the high redox potential around 4.1 V (*vs* Li^+/Li) of Mn^{3+}/Mn^{2+} redox couple [13]. But, the electrochemical performance of LMP is usually hindered by its low electronic conductivity ($\sim 10^{-10}$ S cm^{-1}) and lithium ion diffusion coefficient [13,16]. Fe doping can probably alleviate the Jahn-Teller distortion of Mn^{3+}, stabilize the crystal structure, and enhance electron and lithium ion transfer [14–16]. Yamada et al. reported that olivine-type $Li_x(Mn_{0.6}Fe_{0.4})PO_4$ ($0 \le x \le 1$) delivers a capacity of 160 mAh/g at 0.1 C rate with a high 4 V voltage plateau and low cost [17]. Thus, we choose $LiMn_{0.6}Fe_{0.4}PO_4$ as a cathode in this work, which may show good electrochemical performance by Fe doping.

Recently, triboelectric nanogenerators (TENGs) have drawn much attention for their ability to harvest mechanical energy and convert it into electrical form [18–20]. TENGs can harvest energy from daily human motion to supply energy to energy storage devices such as LIBs,

* Corresponding author.
** Corresponding authors at: CAS Center for Excellence in Nanoscience, Beijing Institute of Nanoenergy and Nanosystems, Chinese Academy of Sciences, Beijing 100083, PR China.
E-mail addresses: ja.alonso@icmm.csic.es (J.A. Alonso), sunchunwen@binn.cas.cn (C. Sun), zhong.wang@mse.gatech.edu (Z.L. Wang).

https://doi.org/10.1016/j.nanoen.2018.08.007
Received 19 May 2018; Received in revised form 18 July 2018; Accepted 4 August 2018
Available online 14 August 2018
2211-2855/

and thus improve their working time. Many efforts have been made to integrate TENGs with various energy storage devices to form self-powered systems [21–23].

Herein, neutron powder diffraction (NPD) investigations on LMP and LMFP were conducted to gain insight into the crystal structural information. The effects of Fe doping on the electrochemical properties of LMP are systematically investigated. The coin cell with LMFP cathode shows good rate capability up to 10 C. This material can be cycled at 1 C rate for over 1000 cycles with Coulombic efficiency higher than 99.5%. In addition, we developed a flexible LIB based on a quasi-solid electrolyte and high voltage LMFP cathode material, which exhibits excellent cycling performance and stability against various deformations. The methyl methacrylate (MMA) based quasi-solid electrolyte not only provides a wide electrochemical window, but also serves as a solid barrier to fasten and protect electrodes. Furthermore, we demonstrated a wearable self-charging power pack by integrating this flexible battery with a flexible TENG to power a flexible electrochromic membrane by harvesting the mechanical energy of various motions of human.

2. Results and discussion

The as-prepared Fe doped $LiMnPO_4$ were firstly examined by X-ray diffraction (XRD) measurements. As shown in Fig. S1, all the peaks in the XRD pattern of $LiMn_{0.6}Fe_{0.4}PO_4$ (LMFP) shows a right shift compared to those of the pristine LMP since the ionic radius of Mn^{2+} (0.66 Å) is larger than that of Fe^{2+} (0.63 Å) [24]. The blue and green lines are pure $LiMnPO_4$ and $LiFePO_4$ respectively, the peaks of the as-prepared LMFP lie between those of LMP and LFP, indicating formation of a pure phase of an olivine solid solution. To further investigate the structure of LMFP, a synchrotron radiation X-ray diffraction (SR-XRD) was employed. Refined SR-XRD pattern and crystal structure of LMFP are shown in Fig. S1b and S1c, respectively. SR-XRD result also indicates formation of a pure phase solid solution. Furthermore, neutron powder diffraction (NPD) data was collected at room temperature (RT) and the crystal structures were refined in order to identify the structural changes introduced in $LiMnPO_4$ upon Fe doping, concerning oxygen coordination and thermal displacement factors, in relation to the evolution in the properties observed in this work. Both of the crystal structures of LMP and LMFP are defined in the orthorhombic *Pnma* (No. 62) space group; the majority of the atoms (Mn, Fe, P, O1 and O2) are located in the special position 4*c*, Li is on the inversion center, 4*a* position, and O3 is in the general 8*d* position. The Rietveld refinement of the structure was performed using, as initial model, the atomic positions published by Rousse et al. [25] In $LiMn_{0.4}Fe_{0.6}PO_4$, Mn and Fe atoms were distributed at random over the same octahedral positions. Li occupancy was also refined and resulted to be stoichiometric within one (LMP) or four (LMFP) standard deviations. The access to a wide region of the reciprocal space allowed us to successfully refine the anisotropic displacement factors for all the atoms, minimizing the correlation with the occupancy factors. The final atomic parameters and occupancy factors together with atomic displacement factors after the full refinement of the crystal structures are included in Tables S1 and S2 for LMFP and LMP, respectively. Fig. 1a and b show the goodness of the neutron fits. Table S3 summarizes the main bond distances after the refinement from NPD data.

It is well known that LMFP, which belongs to the olivine family, presents a triphylite $FePO_4$ type-structure. The olivine corresponds to a structural formula AB_2O_4 where A and B occupy the tetrahedral and octahedral cavities of a HCP oxygen network, respectively. In LMFP, Li and (Mn, Fe) ions are distributed within the octahedral sites in a very different way. Li^+-ions form chains sharing edges and running parallel

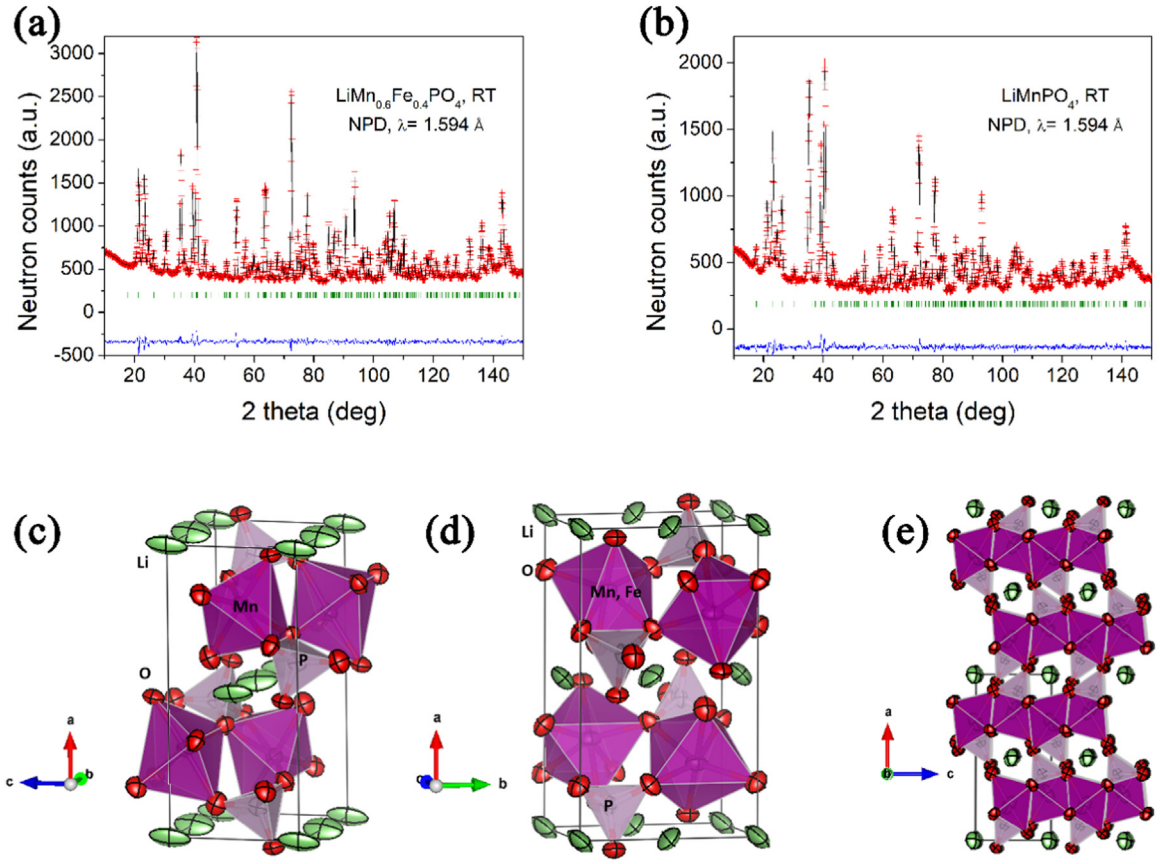

Fig. 1. (a) NPD pattern of the as-synthetised LMFP sample. (b) NPD pattern of the as-synthetised LMP sample. (c) Crystal structure of LMP. (d) Crystal structure of LMFP. (e) Crystal structure of LMFP highlighting the existence of channels along [010] directions that enable the diffusion of Li^+-ions.

to [010] orthorhombic direction (see Fig. 1c for LMP and Fig. 1d for LMFP); each (Mn, Fe)O_6 octahedron is sharing corners with four other (Mn, Fe)O_6 octahedra and with four PO_4 tetrahedra, one of them via one edge. In this structure, tunnels along which Li^+-ions can be removed are identified in the [010] direction, as highlighted in Fig. 1e. Li is connected to 2O1, 2O2 and 2O3 oxygen atoms. A calculation of the bond valence by the Brown's model [26–28] yields valence values close to the expected + 1 for Li^+-ions, as shown in Table S4. Reasonable valence values are also observed for the remaining cations with (Mn, Fe) close to the expected divalent state, and pentavalent for P atoms. For oxygen atoms the anisotropy of the thermal ellipsoids is patent, with the flattened thermal ellipsoids perpendicular to the chemical bonds to (Mn, Fe). It is worth comparing the thermal ellipsoids obtained for lithium atoms in $LiMnPO_4$ with those of $LiMn_{0.6}Fe_{0.4}PO_4$. For the former compound (Fig. 1c) the thermal motion of Li atoms is considerably anisotropic, with prolate cigar-shaped ellipsoids approximately orientated along the [001] directions. The root-mean-square (RMS) displacements of Li are 0.21 Å along the c axis and 0.06 Å perpendicular to it. This is not expected for an ionic conductor where Li ions are anticipated to diffuse along the *b* axis, following the channels determined by PO_4 and MnO_6 polyhedra (see Fig. 1e). This may account for the relatively poor electrochemical performance of $LiMnPO_4$ as cathode material as reported later, since the thermal motion, captured at RT during the NPD experiment, seems to indicate a preference for lithium atoms to vibrate approximately along [001], forced by structural bonding constrains. By contrast, $LiMn_{0.6}Fe_{0.4}PO_4$ exhibits much less anisotropic ellipsoids for Li, with RMS displacements of only 0.12 Å along the *c* axis and 0.08 Å perpendicular to it. The component along the *b*-axis direction is superior, suggesting an easiness for Li to diffuse across the structure, thus implying a significant ionic mobility. A second distinctive feature between both closely related structures is the higher octahedral distortion observed for (Mn, Fe)O_6 in LMFP with respect to MnO_6 octahedra in LMP. The relative distortion can be quantified by the Δ_{oct} parameter, concerning the deviation of (Mn, Fe)-O distances with respect to the average < (Mn, Fe)-O > value, as $\Delta_{oct} = (1/6)\Sigma_{n=1,6}[(d_n - < d >)/< d >]^2$, see Table S3. For $LiMnPO_4$, Δ_d is moderately distorted (9.37×10^{-4}); however this parameter substantially increases for the Fe compound, reaching $\Delta_d = 15.35 \times 10^{-4}$. The origin of this additional distortion is the occurrence of exceptionally short (Mn,Fe)-O2 and (Mn,Fe)-O3 distances of 2.104(7) and 2.094(4) Å (Table S3): these extra bonds to oxygens may weaken the Li-O interactions thus making easier the Li^+-ion diffusion across the structure.

For improving the electronic conductivity, the LMP and LMFP were coated with carbon. The carbon loading is about 11.3%, as shown in Fig. S2. The electrochemical performance of LMP/C and LMFP/C are evaluated by galvanostatic charge/discharge (GCD) tests in coin half-cells with $LiPF_6$ based liquid electrolyte. The cycling and rate performance are shown in Fig. 2. Fig. S3 shows the charge and discharge curves of LMFP/C at different C-rates. As shown in Fig. 3b, compared to the cell with LMP/C cathode, the cell with LMFP/C exhibits better rate performance at higher current densities. The discharge capacity (~90 mAh g^{-1}) of the cell with LMFP/C at 1 C rate is about five times of that of the cell with LMP/C. The cell with LMFP/C can further deliver a capacity of ~50 mAh g^{-1} even at 10 C rate, which is still higher than that of the cell with LMP/C at 1 C rate. It is believed that the doping of Fe^{2+} in LMP can enhance the electronic conductivity and lithium ion diffusion coefficient of the material [13,16,29]. As mentioned above, the NPD results coincide with the higher lithium ion diffusion coefficient in LMFP. The bandgap energy of $LiMnPO_4$ and $LiMn_{0.6}Fe_{0.4}PO_4$ were determined by UV–vis–NIR diffuse reflectance spectra (DRS) via Kubelka – Munk function [30]. The measured bandgap is 3.45 eV and 3.08 eV for LMP and LMFP, respectively, as shown in Fig. S4. A

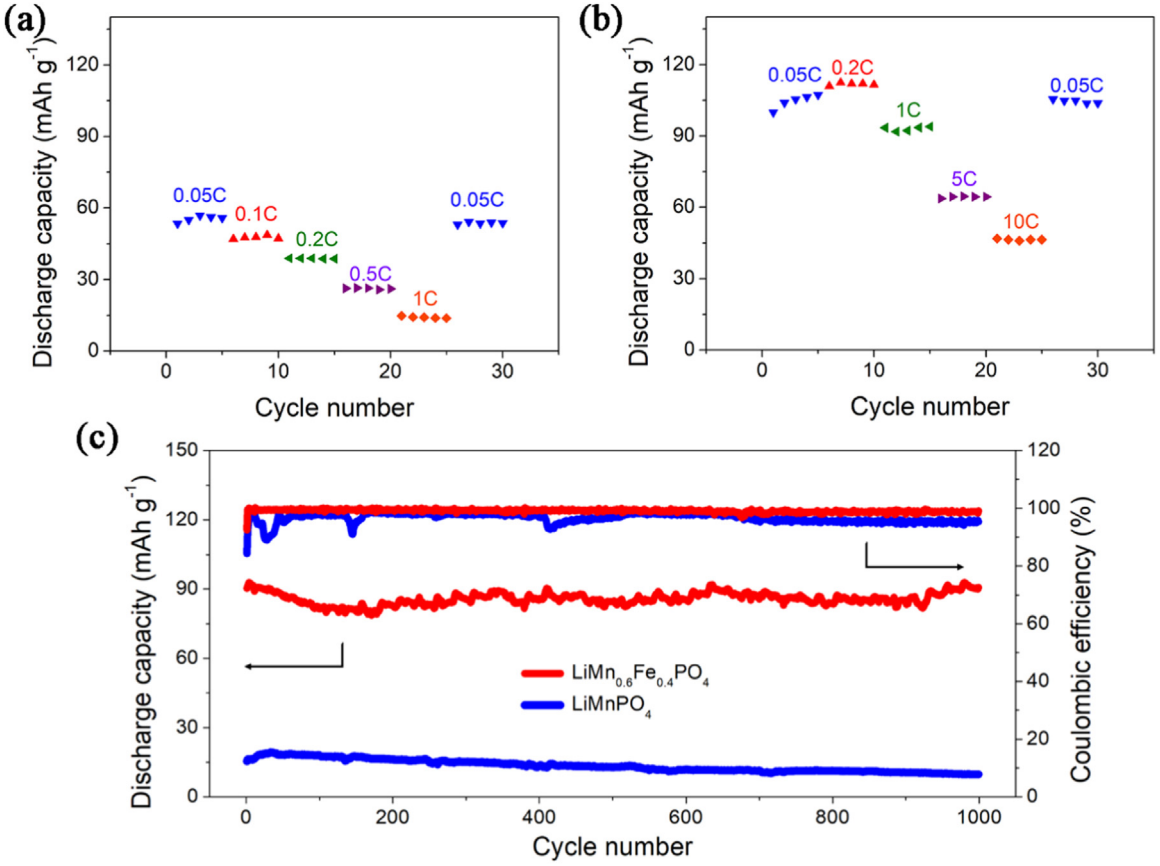

Fig. 2. (a) Rate performance of the cell with LMP/C cathode. (b) Rate performance of the cell with LMFP/C cathode. (c) Discharge capacity and Coulombic efficiency versus cycle number of the cells with LMP/C and LMFP/C cathodes at 1 C rate.

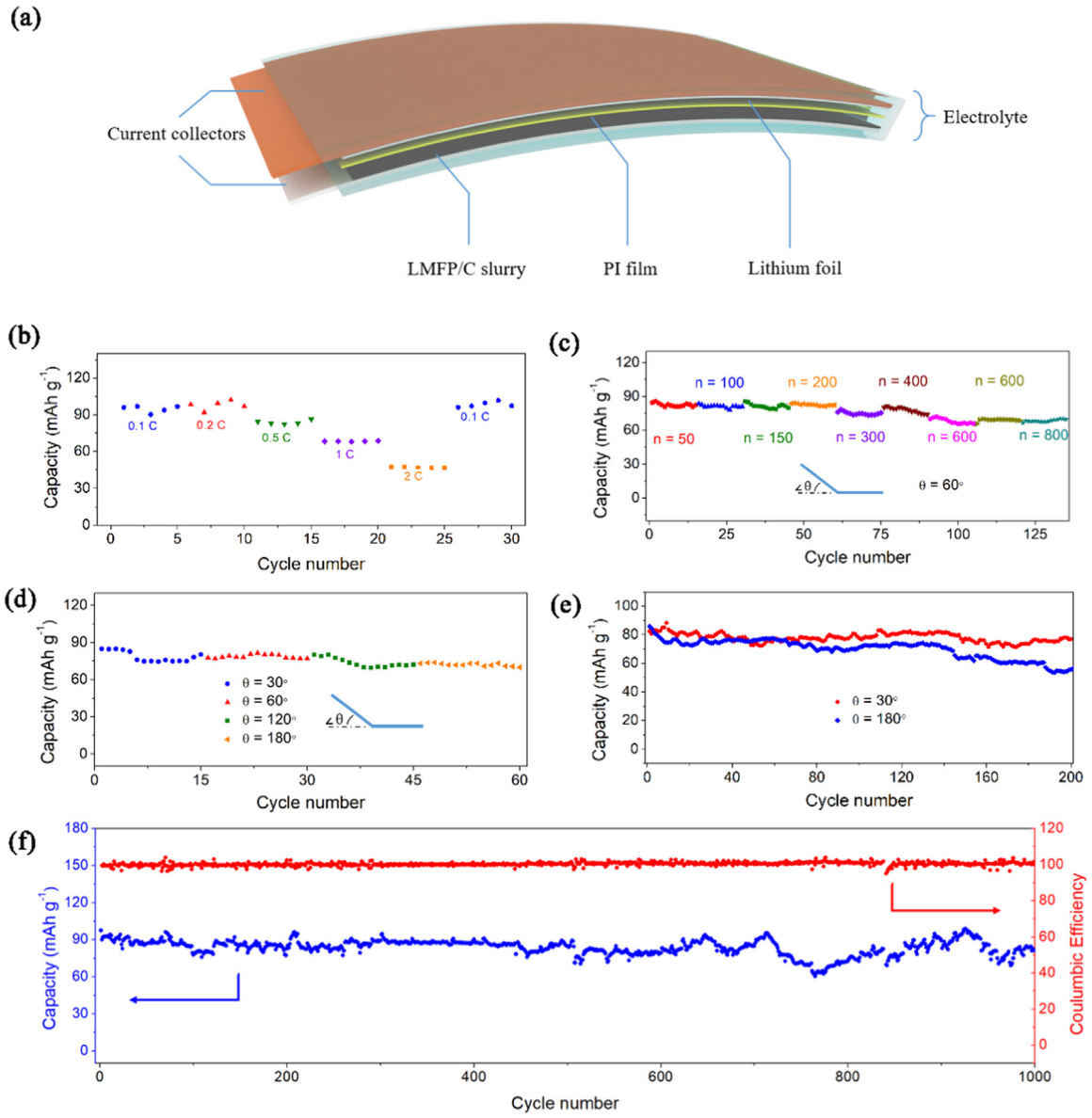

Fig. 3. (a) Schematic of the flexible LIB battery. (b) Rate performance of the flexible cell. (c) Cycling performance of the cell which was bent for different cycles at 0.5 C rate. (d) Cycling performance of the cell at 0.5 C rate and at different bending degrees. (e) Comparison of the cycling performance of the cell at 0.5 C rate under two different deformed states. (f) Cycle performance of the cell under the flat state at 0.5 C rate.

decrease in band gap usually causes higher volume density of conductive electrons, thus leads to higher electronic conductivity and better electrochemical performance at higher current densities. In this study, Fe doping not only improves the rate performance, but also stabilizes the cycling performance. Fig. 2c shows the cycling performance of the cells with LMP/C and LMFP/C materials at 1 C rate. It is observed an obvious capacity fading of the cell with LMP/C. The capacity of the cell with LMP/C decays 37.4% after 1000 cycles. As for the cell with LMFP/C, an average capacity drop is only 1.3% during 1000 cycles at the same current density. The Coulombic efficiency of the cell with LMFP is also enhanced. The cell with the LMFP/C cathode has an average Coulombic efficiency of 99.03% for 1000 cycles while that of the cell with LMP/C is only 96.64%.

A MMA/PI based electrolyte is studied for preparing a flexible battery. As shown in Fig. S5, from the Nyquist plot of EIS test, we can calculate the ionic conductivity of this electrolyte is 1.15×10^{-4} S cm^{-1}. This electrolyte shows a wide electrochemical window up to 5.5 V, owing to the excellent stability of $TFSI^-$ and the complete polymerization of MMA on PI substrate. As shown in Fig. S5b, the current increases sharply at 5.5 V *vs* Li^+/Li, indicating that the electrolyte decomposes at this voltage. The wide electrochemical window enables the polymer to be used as electrolyte for batteries with LMFP cathode. Compared to traditional liquid electrolytes, such as 1 M $LiPF_6$ in EC/DEC electrolyte, this polymer electrolyte can maintain good Coulumbic efficiency at a higher charging voltage. In this case, the Coulumbic efficiency of the flexible cell with LMFP/C and quasi-solid electrolyte reaches 99.9%, higher than that of the coin cell with commercial 1 M $LiPF_6$ EC/DEC electrolyte (99.0%). The lower Coloumbic efficiency of the cell with the commonly used liquid electrolyte might be related to a series of decomposition reactions of $LiPF_6$ since the cut-off charging voltage of LMFP is close to the decomposition voltage of the $LiPF_6$ (~4.5 V *vs* Li^+/Li). In addition, the decomposition products of $LiPF_6$ at high voltage can further react with Mn^{3+} in the presence of trace impurities of water and finally lead to the dissolution of manganese during cycling [31]. However, the MMA/PI/LiTFSI based electrolyte can alleviate these effects.

The overview of the designed flexible cell is schematically shown in Fig. 3a. The rate performance of this flexible cell is a bit lower than that

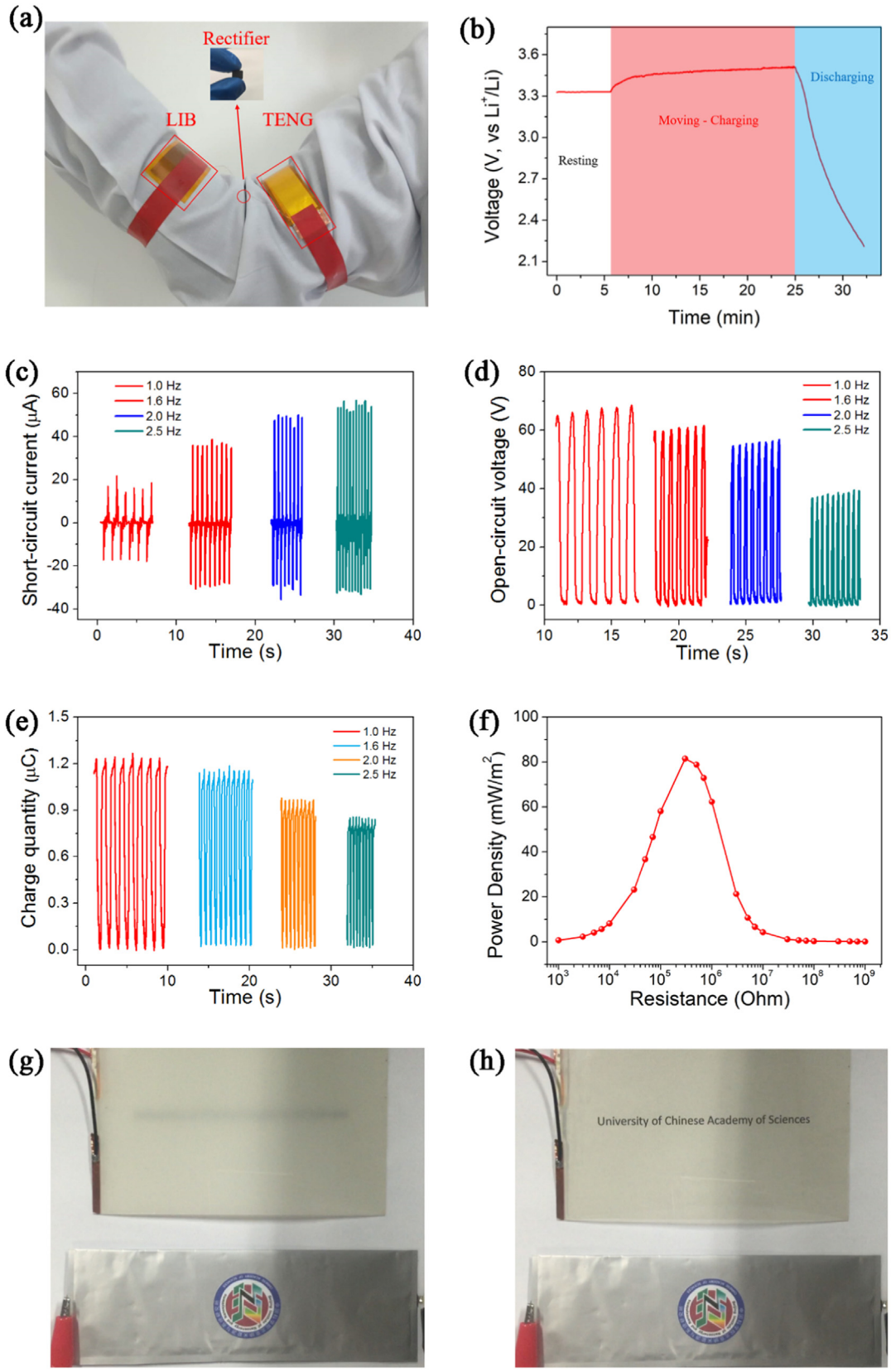

Fig. 4. (a) Photograph of the wearable self-charging power pack consisting of a flexible battery and a flexible TENG. (b) Charge and discharge curves of the flexible LIB. The operator stayed resting in the white region, while the arm of the operator is moving and the battery is charged in the pink region. The battery is discharged in the blue region. (c) Short-circuit current of the flexible TENG at different impact frequencies. (d) Open-circuit voltage of the flexible TENG at different impact frequencies. (e) Charge quantity of the flexible TENG at different impact frequencies. (f) Output power density versus different external load resistances. (g, h) Photographs of the flexible cell powering a flexible electrochromic membrane. (For interpretation of the references to color in this figure legend, the reader is referred to the web version of this article).

of the coin cell with liquid electrolyte, especially at high C rates, as shown in Fig. 3b. This can be attributed to the lower conductivity of the MMA/PI based electrolyte as well as the contact issue of flexible cell. However, the flexible cell with polymer electrolyte shows extraordinary cyclability. The cell can cycle for 1000 cycles at 0.5 C rate in its flat state. After 1000 cycles, the capacity decay of this cell is about 12%, which is better than most flexible LIBs reported in literatures (detail shown in Table S5). As shown in Fig. 3c, the cell can be bent for 800 times. As shown in Table S6, the average capacities of the cell bent for different times are almost not changed. After 800 cycles at bending states, an average retention of the discharge capacity of the cell reaches 82.98%. Moreover, the capacities of the cell bent at different degrees are almost the same, the average discharge capacity decreases only about 8% after bending from 30° to 180°. Fig. 3e compares the cyclability of the cell at two bending states at 0.5 C. It indicates that the cell can work properly at these states for 200 cycles. It should be noted that this cell can be cycled for 500 times under a bending state of 180° state (Fig. S6). The excellent performance of the flexible cell may be attributed to the in-situ polymerized flexible electrolyte between cathode and anode and the packaging design. The fully polymerized electrolyte serves not only as a lithium ion conductor and separator, but also a polymer binder to fix and protect electrodes, ensuring good interface contact of the cell under different deformed states.

The excellent flexibility and good safety of the cell make it potential to be used to power wearable electronics, such as intelligent electronics and sensors [32,33]. However, the energy density of the flexible LIBs is relatively low compared with rigid cells. Increasing the working time of the batteries is important for their practical application [4]. To address this issue, developing a wearable self-charging power pack by integrating flexible cell with a flexible TENG is a possible strategy, as shown in Fig. 4a. TENG can harvest mechanical energy generated by human motions, and convert it into electric energy. Then the flexible LIB further stores the electric energy and powers electronics [34]. Fig. S7 shows the structural schematic diagram of TENG used in this system. As shown in Fig. 4c, the short-circuit current of TENG is about 40 μA at 1.6 Hz, which is similar to that of human motion. At this frequency, the open-circuit voltage is 60 V. Fig. 4f shows output power density versus different external load resistances. A peak is observed at 1 M Ohm. Due to the outstanding flexibility of the LIB, TENG and the light weight of rectifier, the whole system is suitable for powering wearable electronics. Fig. 4b shows a charging curve of LIB in the system, in which the mechanical energy of arm bending is harvested by TENG and the flexible LIB is charged by the TENG. The voltage of the flexible LIB is increased from 3.325 V to 3.50 V in about 20 min. Due to the power limit of TENG, it takes long time to demonstrate the whole charging process. By a simple calculation, if the active area of integrated TENG is 1 m^2, corresponding to the surface area of a child body [35], it will take 7.5 h to fully charge an integrated flexible LIB with 100 mg LMFP by daily human motions. Figs. 4g and h demonstrate the energy system to power a flexible electrochromic membrane. After charging by the TENG, the cell can power the electrochromic membrane, displaying clearly the words below the membrane. Fig. S9a shows that the electrochromic membrane is transparent when it is powered by a flexible cell. After discharging for several hours, the membrane became opaque due to the voltage drop of the cell. Then we charged the cell by integreting flexible TENG through various motions as shown in Fig. S10. After charging about 3 h, the flexible cell can power the membrane again (Fig. S9c). Supplemental videos of this demonstration are also provided.

Supplementary material related to this article can be found online at doi:10.1016/j.nanoen.2018.08.007.

3. Conclusion

The effects of Fe doping on the crystal structure of LMP were systematically investigated by NPD. $LiMn_{0.6}Fe_{0.4}PO_4$ shows superior cyclability for 1000 cycles with no obvious performance drop and good rate capability up to 10 C. The improved electrochemical performance is ascribed to the higher octahedral distortion of (Mn, Fe)O_6 and an easiness for Li diffusion due to much less anisotropic ellipsoids for Li in LMFP. A quasi-solid electrolyte with wide electrochemical window was developed by fully polymerizing MMA on PI substrate. In addition, a flexible LIB was fabricated with $LiMn_{0.6}Fe_{0.4}PO_4$ cathode and PMMA-PI electrolyte, which shows outstanding flexibility and cyclability. The cell can work well under various deformed states for hundreds of cycles. Furthermore, we integrated a flexible TENG with the flexible LIB to demonstrate a prototype of wearable self-charging power pack. A flexible LIB was successfully charged by TENG with human motions, which demonstrates the feasibility of this self-powered system for powering a wearable electronic device.

Acknowledgments

The authors acknowledge the financial support of National Natural Science Foundation of China (Nos. 51672029 and 51372271) and the National Key R & D Project from Ministry of Science and Technology, China (2016YFA0202702). This work was also supported by and the Thousands Talents Program for the pioneer researcher and his innovation team in China. J. A. A. gratefully acknowledges the Spanish Ministry of Economy and Competitivity for granting the project MAT2017-84496-R, ALBA for providing synchrotron x-ray beam time and ILL for making all facilities available for the neutron diffraction experiments.

Appendix A. Supporting information

Supplementary data associated with this article can be found in the online version at doi:10.1016/j.nanoen.2018.08.007.

References

[1] J. Zhu, L. Chen, Z. Xu, B. Lu, Nano Energy 12 (2015) 339–346.
[2] S. Song, R. Hill, K. Choi, K. Wojciechowski, S.J. Leisen, H.J. Snaith, S.R. Marder, T. Park, Nano Energy 49 (2018) 324–332.
[3] Y. Zhang, C.K. Jeong, J. Wang, H. Sun, F. Li, G. Zhang, L. Chen, S. Zhang, W. Chen, Q. Wang, Nano Energy 50 (2018) 35–42.
[4] H. Cha, J. Kim, Y. Lee, J. Cho, M. Park, Small 13 (2017) 1702989–1703006.
[5] M. Stoppa, A. Chiolerio, Sensors 14 (2014) 11957–11992.
[6] M. Armand, J.M. Tarascon, Nature 451 (2008) 652–657.
[7] N.S. Choi, Z. Chen, S.A. Freunberger, X. Ji, Y.K. Sun, K. Amine, G. Yushin, L.F. Nazar, J. Cho, P.G. Bruce, Angew. Chem. Int. Ed. 51 (2012) 9994–10024.
[8] Z. Zhang, M. Liao, H. Lou, Y. Hu, X. Sun, H. Peng, Adv. Mater. 30 (2018) 1704261–1704279.
[9] A.J. Blake, R.R. Kohlmeyer, L.F. Drummy, J.S. Gutiérrez-Kolar, J. Carpena-Núñez, B. Maruyama, R. Shahbazian-Yassar, H. Huang, M.F. Durstock, ACS Appl. Mater. Interfaces 8 (2016) 5196–5204.
[10] K.K. Fu, J. Cheng, T. Li, L. Hu, ACS Energy Lett. 1 (2016) 1065–1079.
[11] A.K. Pahdi, K.S. Nanjundaswamy, J.B. Goodenough, J. Electrochem. Soc. 144 (1997) 1188–1194.
[12] C. Sun, S. Rajasekhara, J.B. Goodenough, F. Zhou, J. Am. Chem. Soc. 133 (2011) 2132–2135.
[13] M.K. Devaraju, I. Honma, Adv. Energy Mater. 2 (2012) 284–297.
[14] L.F.J. Piper, N.F. Quackenbush, S. Sallis, D.O. Scanlon, G.W. Watson, K.W. Nam, X.Q. Yang, K.E. Smith, F. Omenya, N.A. Chernova, M.S. Whittingham, J. Phys. Chem. C 117 (2013) 10383–10396.
[15] C.A. Burba, R. Frech, J. Power Sources 172 (2007) 870–876.
[16] M. Yonemura, A. Yamada, Y. Takei, N. Sonoyama, R. Kanno, J. Electrochem. Soc. 151 (2004) A1352–A1356.
[17] A. Yamada, Y. Kudo, K.Y. Liu, J. Electrochem. Soc. 148 (2001) A747–A754.
[18] Z.L. Wang, Mater. Today 20 (2017) 74–82.
[19] Z.L. Wang, Faraday Discuss. 176 (2014) 447–458.
[20] Z.L. Wang, ACS Nano 7 (2013) 9533–9577.
[21] H.D. Hou, Q.K. Xu, Y.K. Pang, L. Li, J.L. Wang, C. Zhang, Z.L. Wang, Adv. Sci. 4 (2017) 1700072–1700076.
[22] X. Zhang, X. Du, Y. Yin, N.W. Li, W. Fan, R. Cao, W. Xu, C. Zhang, C. Li, ACS Appl. Mater. Interfaces 10 (2018) 8676–8684.
[23] H. Guo, M.H. Yeh, Y. Zi, Z. Wen, J. Chen, G. Liu, C. Hu, Z.L. Wang, ACS Nano 11 (2017) 4475–4482.
[24] R.D. Shannon, Acta Cryst. A32 (1976) 751–767.
[25] G. Rousse, J. Rodriguez-Carvajal, S. Patoux, C. Masquelier, Chem. Mater. 15 (2003) 4082–4090.

[26] M. O'Keeffe, A. Navrotsky, In Structure and Bonding in Crystals, Academic Press, New York, 1981, pp. xiii–xv.
[27] N.E. Brese, M. O'Keeffe, Acta Crystallogr. B 47 (1991) 192–197.
[28] I.D. Brown, Z. Krist. 199 (1992) 255–272.
[29] P. Kubelka, K. Munk, Z. Technol, Phys 11a (1931) 593–603.
[30] W.F. Huang, S. Tao, J. Zhou, C. Si, X. Chen, W. Huang, C.H. Jin, W.S. Chu, L. Song, Z.Y. Wu, J. Phys. Chem. C 118 (2014) 796–803.
[31] K. Kleiner, H. Ehrenberg, Top. Curr. Chem. 375 (2017) 54–98.
[32] W. Zeng, L. Shu, Q. Li, S. Chen, F. Wang, X.M. Tao, Adv. Mater. 26 (2014) 5310–5336.
[33] W. Gao, S. Emaminejad, H.Y.Y. Nyein, S. Challa, K. Chen, A. Peck, H.M. Fahad, H. Ota, H. Shiraki, D. Kiriya, D.H. Lien, G.A. Brooks, R.W. Davis, A. Javey, Nature 529 (2016) 509–514.
[34] K. Zhao, Y. Yang, X. Liu, Z.L. Wang, Adv. Energy Mater. 7 (2017) 1700103–1700110.
[35] J.F. Wang, E. Hihara, Eur. J. Appl. Physiol. 92 (2004) 13–17.

Shaoqing Li received his Bachelor's Degree from Beijing Institute of Technology in 2015. He is currently a Master candidate in Condensed Matter Physics under the supervision of Professor Chunwen Sun at Beijing Institute of Nanoenergy and Nanosystems (BINN), Chinese Academy of Sciences (CAS). His current research interests focus on flexible rechargeable batteries.

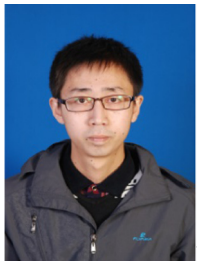

Xiaoyi Meng received his Bachelor's Degree in Chemical Biology from Tianjin Normal University. He is currently a Ph.D. candidate under the supervision of Professor Chunwen Sun at Beijing Institute of Nanoenergy and Nanosystems (BINN), Chinese Academy of Sciences (CAS). His current research interests focus on high performance metal-air batteries, electrochemical catalysis, TENG-based sensors.

Qiang Yi received his Bachelor's Degree from Hefei University of Technology in 2016. He is currently a Master candidate in Physical Chemistry under the supervision of Professor Chunwen Sun at Beijing Institute of Nanoenergy and Nanosystems (BINN), Chinese Academy of Sciences (CAS). His current research interests focus on polymer-based electrolyte for rechargeable batteries.

Prof. José Antonio Alonso is a professor of research in Instituto de Ciencia de Materiales de Madrid de Madrid, CSIC, Spain. His research interests include high-pressure synthesis of transition metal oxides with unusual electronic and magnetic properties, such as metal-insulator transitions, superconductivity or colossal magnetoresistance. Energy conversion and storage materials, in particular oxide materials for solid-oxide fuel cells (SOFC) and intermetallic alloys for hydrogen storage and thermoelectric materials. Frequent user of neutron diffraction techniques applied to the determination of crystal and magnetic structures. In UT-Austin he worked in the design and development of new electrode and electrolyte materials for SOFC.

Maria Teresa Fernandez-Diaz is the Head of the Diffraction Group at the Institut Laue Langevin in Grenoble. She received her Ph.D. in Solid State Physics at the University Autonoma of Madrid, followed by a postdoctoral fellowship at the Laboratoire Leon Brillouin in Saclay. She was after appointed as Instrument Scientist at the ILL and acquired a large experience in neutron diffraction techniques in powder and single-crystal. Her scientific interest lies mainly in the field of structural and magnetic aspects of oxides presenting charge, spin and orbital ordering phenomena. Progressively she has broadened her interests to different energy related materials as well as to magnetic ionic liquids.

Prof. Chunwen Sun received his Ph.D. degree in Condensed Matter Physics from the Institute of Physics (IOP), Chinese Academy of Sciences (CAS) in 2006. He is a full professor and group leader of Energy Storage Materials and Devices at Beijing Institute of Nanoenergy and Nanosystems (BINN), CAS. His research interests include energy storage and conversion, e.g., lithium-ion batteries, metal-air batteries, all-solid-state batteries, fuel cells and self-powered systems. He has published 90 peer-reviewed papers with a citation more than 4000 times, edited 5 book chapters and filed 15 Chinese patents. He has also received a number of awards, including the Outstanding Overseas Talents by the Institute of Physics CAS (2011), the Second Prize of Military Progress Prize in Science and Technology Advancement in China (2013) and the International Association of Advanced Materials (IAAM) Scientist Medal (2017).

Prof. Zhong Lin (ZL) Wang received his Ph.D. from Arizona State University in physics. He now is the Hightower Chair in Materials Science and Engineering, Regents' Professor, Engineering Distinguished Professor and Director, Center for Nanostructure Characterization, at Georgia Tech. Dr. Wang has made original and innovative contributions to the synthesis, discovery, characterization and understanding of fundamental physical properties of oxide nanobelts and nanowires, as well as applications of nanowires in energy sciences, electronics, optoelectronics and biological science. His discovery and breakthroughs in developing nanogenerators established the principle and technological road map for harvesting mechanical energy from environment and biological systems for powering a personal electronics. His research on self-powered nanosystems has inspired the worldwide effort in academia and industry for studying energy for micro-nano-systems, which is now a distinct disciplinary in energy research and future sensor networks. He coined and pioneered the field of piezotronics and piezo-phototronics by introducing piezoelectric potential gated charge transport process in fabricating new electronic and optoelectronic devices.